Lehrstuhl für Bildverarbeitung
Institute of Imaging & Computer Vision

Modeling and Compensation of Geometric Distortions of Multispectral Cameras with Optical Bandpass Filter Wheels

Johannes Brauers and Nils Schulte and Til Aach
Institute of Imaging and Computer Vision
RWTH Aachen University, 52056 Aachen, Germany
tel: +49 241 80 27860, fax: +49 241 80 22200
web: www.lfb.rwth-aachen.de

in: 15th European Signal Processing Conference. See also BibTeX entry below.

BibTeX:

```
@article{Brauers2007,
  author      = {Johannes Brauers and Nils Schulte and Til Aach},
  title       = {Modeling and Compensation of Geometric Distortions of Multispectral
                 Cameras with Optical Bandpass Filter Wheels},
  booktitle   = {15th European Signal Processing Conference},
  publisher   = {EURASIP},
  pages       = {1902--1906},
  year        = {2007},
  address     = {Pozna\'{n}, Poland},
  month       = {Sep}
}
```


document created on: December 2, 2008
created from file: main.tex
cover page automatically created with CoverPage.sty
(available at your favourite CTAN mirror)

RWTH AACHEN
RHEINISCH-WESTFÄLISCHE TECHNISCHE HOCHSCHULE AACHEN

MODELING AND COMPENSATION OF GEOMETRIC DISTORTIONS OF MULTISPECTRAL CAMERAS WITH OPTICAL BANDPASS FILTER WHEELS

Johannes Brauers, Nils Schulte, and Til Aach

Institute of Imaging & Computer Vision, RWTH Aachen University
D-52056 Aachen, Germany
phone: +49 241 80-27866, email: jb,ta@lfb.rwth-aachen.de
web: www.lfb.rwth-aachen.de

ABSTRACT

High-fidelity colour reproduction requires multispectral cameras for image acquisition, which, unlike RGB cameras, divide the visible electromagnetic spectrum into more than 3 channels. This can be achieved by successively placing narrow-band optical filters with different passbands between object lens and sensor of a standard b/w camera. The filters are arranged on a filter wheel, the rotation of which moves the filters sequentially into the optical path. In practice, these filters exhibit different thicknesses and refraction indices, and are also not perfectly coplanar, resulting in geometric distortions between the recorded spectral components. We derive a mathematical model for these distortions. We additionally measure the effects of chromatic aberration, and incorporate these into our model. Based on this model, we then develop a registration algorithm which robustly estimates the parameters of an appropriate affine coordinate transformation. Experimental results using a seven-channel multispectral camera confirm both the validity of our model as well as the accuracy of the registration algorithm.

1. INTRODUCTION

Multispectral cameras provide a much higher colour fidelity [10] than common RGB cameras. The latter ones are available as consumer and professional cameras, ranging from cameras in mobile phones to industrial inspection cameras. Despite their popularity, they produce a systematic colour error since they violate the Luther condition [11], which, for faithful colour reproduction, requires the spectral sensitivities of the 3 colour channels to be a linear combination of those of the CIE standard observer. Especially single-chip RGB cameras using a colour filter array perform poorly in this respect, since they require spatial interpolation within the colour components — often referred to as demosaicking [8] — which generates additional colour errors.

In many multispectral scenarios, the scenes to be acquired are static. One way to achieve multispectral acquisition then is to divide the incoming visible electromagnetic spectrum into a higher number of channels — say, seven — by successively placing optical narrow-band filters with different passbands between object lens and sensor of a standard b/w camera, and to acquire a separate colour component for each filter. Towards this end, the set of filters is mounted on a filter wheel [9, 5], the rotation of which sequentially moves each filter into the optical path (see Fig. 1). The filters sample the spectrum from 400nm to 700nm at discrete intervals in steps of, for instance, 50nm. This makes it possible to differentiate between metamere colours, i.e., colours which appear identical for a specific viewer or RGB camera, but are caused by different reflected spectra. An additional advantage of the multispectral approach is the possibility to generate from *one* given acquisition reproductions for *different* illumination sources with differing properties. Though we focus here on multispectral cameras with filter wheels, let us mention that other techniques exist, such as line scanning [2] or the usage of a liquid crystal tunable filter (LCTF) [1].

In practice, filter wheels exhibit certain imperfections: First, the filters in a wheel are not perfectly coplanar, rather, the normal of each filter is tilted by an individual angle γ with respect to the optical axis, as shown in Fig. 2. Moreover, their thicknesses and refraction indices differ. This generates systematic misalignments between the acquired spectral components, which, when uncompensated, produce colour fringes. Our objective in this contribution is to mathematically model these distortions, and to develop an algorithm consistent with our model to compensate them.

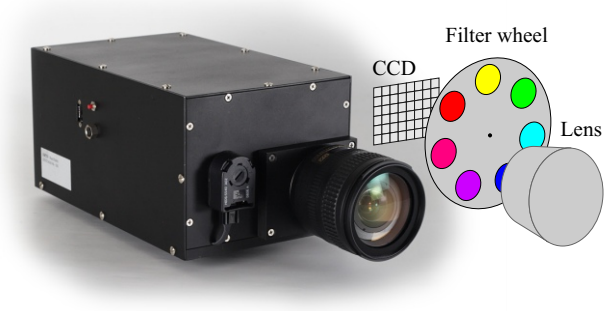

Figure 1: Our multispectral camera, using 7 optical filters. Its internal configuration is sketched.

A region-based registration algorithm using correlation analysis for the correction of ”geometric inter-channel distortions“ of multispectral cameras is described in [9]. But since there is no underlying model, the correction fails in regions without any or with corrupted registration information. Also, the correlation-based similarity measure is not ideally suited because the values of different spectral channels are generally related non-linearly. In [4], an ”automatic registration algorithm“ is proposed, performing registration by a heuristic search of model parameters. Neither the physical background nor the effect of chromatic aberration were analyzed. No comparison between a model estimate and measured data is given.

In the following, we first develop the physical model describing the geometric distortions in multispectral cameras

with filter wheels. Based on the model, we then derive our registration algorithm in section 3. Experimental results with our 7-channel multispectral camera are provided in section 4 before we conclude with section 5.

2. PHYSICAL MODEL

Fig. 2 shows schematically a filter of thickness d and refraction index n_2 placed into the optical path. Its normal is tilted by a small angle γ away from the optical axis. A principal ray incident under the angle θ with respect to the optical axis is refracted twice such that it emerges parallel to its unrefracted path, but is displaced by δ, resulting in the displacement e in the image plane. Since γ, d and n_2 vary from filter to filter, so do the displacements δ and e. The resulting misalignments between the colour channels then generate colour fringes, as observed in Fig. 4 (left). The angle α between the incident ray and the filter normal is

$$\alpha = \theta + \gamma. \tag{1}$$

The refraction obeys Snellius rule

$$\frac{\sin\alpha}{\sin\beta} = \frac{n_2}{n_1} = n_2 \ , \tag{2}$$

where $n_1 = 1$ is the refraction index of air. The displacement δ thus is

$$\delta = d\,\frac{\sin(\alpha-\beta)}{\cos\beta}. \tag{3}$$

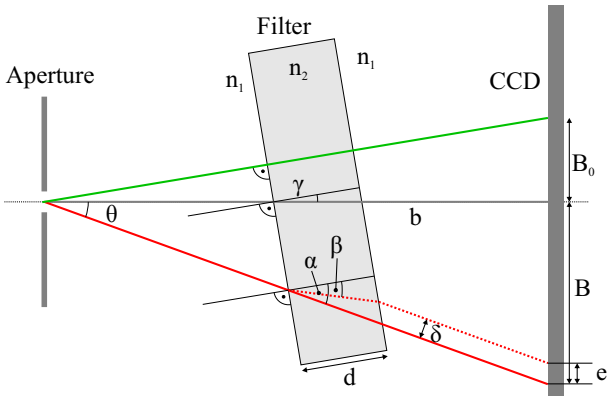

Figure 2: A filter placed between lens (not shown) and sensor, tilted by γ with respect to the optical axis. The filter refracts the ray depicted in solid red as shown by the red dotted line. The ray with $\theta = -\gamma$ (green) is not refracted.

For the displacement in the image plane, we obtain

$$e = \frac{\delta}{\cos\theta}. \tag{4}$$

Combining (2)-(4) yields

$$e = d\,\frac{\sin(\alpha-\beta)}{\cos\beta\cos\theta} \tag{5}$$

Practically, γ is less than $0.5°$. For our filter set, the refraction index is either $n_2 = 1.45$ (for the filters with centre wavelengths 400nm and 450nm), or $n_2 = 2.05$ (for the filters with centre wavelengths 500nm, 550nm, 600nm, 650nm and 700nm). The image distance b is not less than 50mm, and the sensor size is 6.4mm × 4.8mm, yielding a maximum angle $\theta = \pm 3.7°$.

Invoking the trigonometric approximations $\sin x \approx x$, $\cos x \approx 1$ for small angles [1], we simplify (5) to

$$e = d\,(\alpha-\beta). \tag{6}$$

Calculating β by Snellius' rule (2) to

$$\beta = \arcsin\left(\frac{\sin\alpha}{n_2}\right) \approx \frac{\alpha}{n_2} \tag{7}$$

and inserting (1) we obtain for e

$$\begin{aligned} e &= d\left(\theta+\gamma-\frac{\alpha}{n_2}\right) = d\left(\theta+\gamma-\frac{\theta+\gamma}{n_2}\right) \\ &= d\left(1-\frac{1}{n_2}\right)(\theta+\gamma). \end{aligned} \tag{8}$$

From the image distance b and the position B, we find

$$\tan\theta = \frac{B}{b} \approx \theta \tag{9}$$

yielding for the displacement e

$$e = \underbrace{d\left(1-\frac{1}{n_2}\right)}_{C}\left(\frac{B}{b}+\gamma\right) \tag{10}$$

which is a linear relation between the displacement e in the image plane and the filter parameters d, n_2 and γ. To assess the validity of the small-angle approximations, we performed a worst-case comparison between e as computed from (10) and its non-approximated counterpart, which resulted in a maximum discrepancy of only 0.04 pixels, thus confirming the validity of (10). Eq. (10) also allows to find the principal ray which is not refracted, i.e., the angle $\theta \approx B/b$ for which $e = 0$: This is the case for $\theta \approx B_0/b = -\gamma$. This ray impinges on the filter with $\alpha = 0$, as illustrated in Fig. 2. For an ideally aligned filter, i.e. $\gamma = 0$, the displacement e depends multiplicatively on the filter thickness d and the factor $1 - 1/n_2$ determined by the refraction index n_2. In the following, these are summarized in the single factor C.

For two filters with angles γ_i and parameters $C_i = d_i(1 - 1/n_i)$, $i = 1,2$, the difference $\Delta\tilde{e} = e_1 - e_2$ between their respective displacements e_1 and e_2 in the image plane is

$$\Delta\tilde{e} = \left(\frac{B}{b}+\gamma_1\right)C_1 - \left(\frac{B}{b}+\gamma_2\right)C_2 \ . \tag{11}$$

Rewriting (11) yields the linear equation

$$\begin{aligned} \Delta\tilde{e} &= B\underbrace{\frac{1}{b}(C_1-C_2)}_{f} \underbrace{+C_1\gamma_1 - C_2\gamma_2}_{t} \\ &= Bf + t \end{aligned} \tag{12}$$

[1] Note that all angles in the equations are interpreted in radian.

on which we will later base the registration algorithm. Eq. (12) shows that the filter orientation angles γ_i generate a translation vector field with displacements $t = C_1\gamma_1 - C_2\gamma_2$, which do not depend on the position B in the image plane. The position dependent part is caused by differences of the variables C_1 and C_2, i.e. variations in filter thickness and refraction index. Note that the distortion effect of the filters is separable and can be modeled independently for the x- and y-coordinates because Snellius rule can be applied separately for each dimension, which then results in two-dimensional displacement vectors.

We have also investigated the chromatic aberration (CA) of our lens: CA causes a wavelength dependent pincushion or barrel distortion of the image [14], to which the separation of spatial coordinates (x,y) is not applicable since this additional distortion is circular. Later on, we take this into account by using cross coordinate terms, i.e. $x' = f(x,y)$, where (x,y) is a reference point and (x',y') is the corresponding distorted point (see section 3). As also described later in section 4, we have measured the displacements caused by chromatic aberrations alone (see Fig. 7), which are below 0.2 pixels.

3. REGISTRATION

The aim of image registration is to compensate the geometric distortions between the colour components recorded via the different optical filters. Simultaneously, an analysis of the displacement fields enables us to verify our physical model.

The similarity measurement of our registration algorithm is based on mutual information (MI) [13], [12]. Its advantage over other similarity measures such as cross correlation is that MI can still be applied when the values in the reference image and the image to be registered are related by some nonlinear relationship, as it may be the case in our application due to the nonlinear camera transfer function [3] and an otherwise nonlinear behaviour between the spectral channels.

The basic idea behind the MI based similarity measurement is the maximization of the mutual information

$$\begin{aligned}\tilde{\mathbf{v}} &= \operatorname*{argmax}_{\mathbf{v}} I(\mathbf{v}) \\ &= \operatorname*{argmax}_{\mathbf{v}} \sum_{f,r} p_{FR,\mathbf{v}}(f,r) \log_2 \frac{p_{FR,\mathbf{v}}(f,r)}{p_{F,\mathbf{v}}(f)\,p_R(r)}\end{aligned} \tag{13}$$

between the reference region R and the region F to be aligned, which is shifted by $\mathbf{v} = (dx,dy)$. The probability density functions are estimated from the region-internal values using histograms (region size: 96×96 pixels).

We obtain subpixel accuracy by interpolation of the mutual information "surface" around the pixel-precise maximum with a 2nd order two-dimensional polynomial

$$I(dx,dy) = A_1 + A_2 dx + A_3 dy + A_4 dxdy + A_5 dx^2 + A_6 dy^2 \tag{14}$$

and compute the exact maximum analytically. The parameters $A_1,\ldots,A_6$ are obtained by fitting the polynomial to the MI surface values of the positions in the 3×3 neighbourhood of the pixel-precise maximum. We compared the resulting displacement estimates with the results of a subpixel-accurate search, showing that we achieve virtually the same accuracy at significantly shorter processing times.

This unconstrained search procedure with subsequent subpixel refinement is carried out for nonoverlapping regions, and provides a displacement vector field $\mathbf{V} = \{\mathbf{v}(x,y)\}$ with one vector $\mathbf{v}(x,y)$ for each region. This field is used to initialize an iterative computation of an affine transform between the two colour components. The parametric form of the affine transform is based on the mathematical model of the misalignments derived in the previous section, viz., Eq. (12) applied separately to each displacement vector component. Additionally, the multiplicative cross terms introduced by chromatic aberrations are taken into account.

Motivated by the physical model, we use the affine model

$$\begin{pmatrix} x' & y' \end{pmatrix} = \begin{pmatrix} x & y & 1 \end{pmatrix} \mathbf{T} \tag{15}$$

with

$$\mathbf{T} = \begin{pmatrix} f_{00} & f_{01} \\ f_{10} & f_{11} \\ t_x & t_y \end{pmatrix} \tag{16}$$

to capture the relation between a point $\mathbf{x} = (x,y)$ in one colour component and its correspondence $\mathbf{x}'$ in the other component, thus describing the displacement vector field in a manner consistent with our model. In the matrix $\mathbf{T}$, the entries f_{00} and f_{11} depend mainly on the quantity f in (12) as evaluated for each x- and y-dimension, while the elements f_{01} and f_{10} are, in our model, determined by chromatic aberrations. The translation components t_x and t_y in the last row are determined by t in (12), again evaluated separately for the x- and y-dimensions. (As indicated by Fig. 2, our model assumes the origin of the image coordinates to lie in the (unknown) image centre, i.e., the intersection of the optical axis with the image plane. In our implementation, the origin is in the left upper corner. As seen from (12), the resulting coordinate shift is only scaled by the parameter f, and can thus be integrated into the translation t without altering the parametric form of transform (16)). To robustly estimate the transform parameters, and to remove outliers in the initial unconstrained displacement field from the estimation process, we apply the RANSAC [6], [7] algorithm, which is able to estimate the model parameters even when the initial unconstrained field exhibits considerable errors, as in, e.g., Fig. 6.

An alternative approach would be to estimate the six parameters of the affine model directly from the two colour components by an iterative, MI-based registration algorithm evaluating the entire data — rather than only smaller regions — in each step. The downside of doing so is that this would require a search in a six-dimensional parameter space, with each step necessitating the comparison of all available data. In our region-based approach, it suffices to perform the computationally expensive comparison of image data over only two parameters, viz., the translation vector components. The transform parameters are then estimated from the initial vector field $\mathbf{V}$, which, as mentioned above, contains only as many vectors as there are (nonoverlapping) regions.

Our full displacement estimation algorithm is illustrated in Fig. 3. After computing the initial vector field $\mathbf{V}$, we randomly select three point pairs $\mathbf{x}_0,\mathbf{x}'_0$, $\mathbf{x}_1,\mathbf{x}'_1$ and $\mathbf{x}_2,\mathbf{x}'_2$ from this vector field, since three points pairs are required to estimate the transformation matrix $\mathbf{T}$. Using the notations

$$\mathbf{x} = \begin{pmatrix} x & y & 1 \end{pmatrix} \qquad \mathbf{x}' = \begin{pmatrix} x' & y' \end{pmatrix} \tag{17}$$

and

$$\mathbf{X_S} = \begin{pmatrix} \mathbf{x}_0 & \mathbf{x}_1 & \mathbf{x}_2 \end{pmatrix}^T \qquad \mathbf{X'_S} = \begin{pmatrix} \mathbf{x'}_0 & \mathbf{x'}_1 & \mathbf{x'}_2 \end{pmatrix}^T \tag{18}$$

we find the transformation matrix

$$\tilde{\mathbf{T}} = \mathbf{X_S}^{-1}\mathbf{X'_S} \tag{19}$$

for cases where $\det(\mathbf{X_S}) \neq 0$. When $\det(\mathbf{X_S}) = 0$, the selected set of points is degenerate, and another set of point pairs is selected.

In the next step, the quality of the tentative transform estimate $\tilde{\mathbf{T}}$ is assessed by applying it to all points $\mathbf{x_i}$ in the initial vector field. Each point $\mathbf{x_i}$ is transformed by $\tilde{\mathbf{T}}$ according to $\mathbf{x_i}\tilde{\mathbf{T}}$, and compared to its counterpart $\mathbf{x'_i}$ as determined by the initial vector field $\mathbf{V}$. If the distance

$$d_i = \left| \mathbf{x_i}\tilde{\mathbf{T}} - \mathbf{x'_i} \right| \tag{20}$$

is less than a threshold τ (typical value: $\tau = 0.5$ pixel), the corresponding displacement between $\mathbf{x_i}$ and $\mathbf{x'_i}$ is regarded as a consensus vector. The number $P(\tilde{\mathbf{T}})$ of consensus vectors thus obtained for this transformation is then taken to assess the quality of $\tilde{\mathbf{T}}$ — it is supposed to be small if the chosen input points for model estimation are erroneous and large if there is a large consensus.

The procedure is repeated several times and the best model estimate $\tilde{\mathbf{T}}$ is retained. In the final step, this estimate is refined by re-estimating it from all its consensus vectors according to

$$\mathbf{T} = \mathbf{X_P}^{+}\mathbf{X'_P} \tag{21}$$

where $()^+$ denotes the pseudoinverse, and $\mathbf{X_P}$ and $\mathbf{X'_P}$ are formed similarly as in (18), but by now collecting all point pairs linked by consensus vectors.

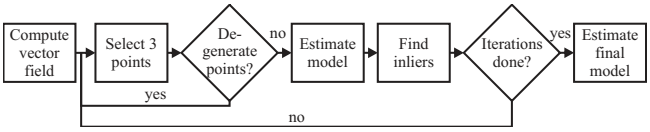

Figure 3: Block diagram of the registration algorithm.

4. EXPERIMENTAL RESULTS

We use a multispectral camera (see Fig. 1) with a 7-channel filter wheel. Internally the camera uses a Sony XCD-SX900 CCD camera with a resolution of 1280×960 pixels. The lens is a Nikkor AF-S DX 18-70mm. Without distortion compensation, the recorded images exhibit rainbow-like edges, as shown in Fig. 4 (left). The colour components are displaced by up to ± 10 pixels with respect to each other. After registration by our model-based algorithm, the colour fringes vanish completely, as shown in Fig. 4 (right).

To verify our model, we acquired a multispectral image of graph paper shown in Fig. 5. We selected the 550nm channel as a reference since it has the best signal to noise ratio, and is the centre channel of our system. The maximum displacement vector length in Fig. 5 is 2.02 pixels. The mean

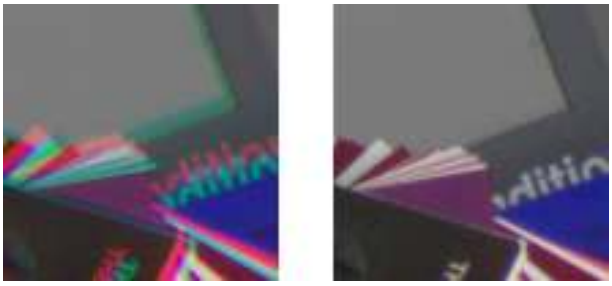

Figure 4: Image before (left) and after (right) registration.

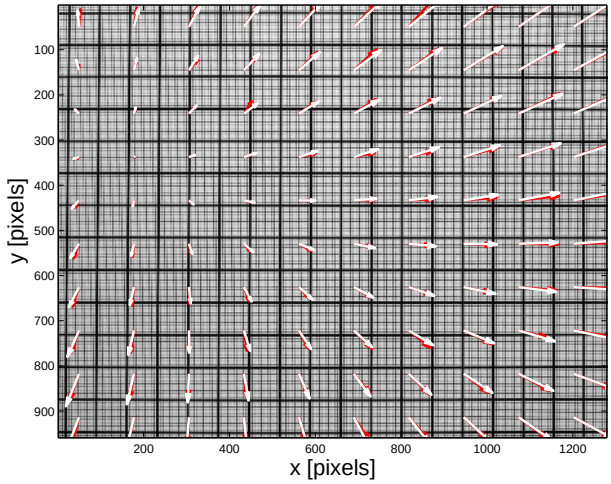

Figure 5: Scaled displacement vector field between channel 3 (500nm) and channel 4 (550nm), red: measurement data, white: model data, maximum vector length: 2.02 pixel, background: spectral channel at 500nm.

error between the measurement vector data and model vector data is only 0.11 pixel, which is below what is noticeable in the final registered image.

Another example image is shown in Fig. 6. In some regions such as homogeneous areas, the initial unconstrained registration algorithm fails and provides vastly erroneous vector estimates. Invoking our mathematical model as described eliminates these stochastic errors. Experiments have shown that the model parameters can still be estimated when more than 80 percent of the data are disturbed by stochastic errors. The estimated transform parameters were $f_{00} = 1.0024$, $f_{11} = 1.0029$, $f_{10} = f_{01} = -0.0006$, and $t_x = -0.4182$, $t_y = -0.8347$, thus showing that chromatic aberration plays a less prominent — though not negligible — role in comparison to the optical bandpass filters. 15 iterations were carried out, and 70 consensus vectors were selected out of 100 vectors.

To measure the effects of chromatic aberration of the Nikon lens, we acquired two images, both with the same optical bandpass filter (centre wavelength: $\lambda_0 = 550$nm) selected within the camera. For the first image, an additional narrow-band optical filter with centre wavelength $\lambda = 500$nm was positioned *in front of the light source*, while for the second image, another optical filter with centre wavelength $\lambda = 600$nm was used. Since these filters have a bandwidth of $\Delta\lambda = 40$nm, their passbands overlap with the passband

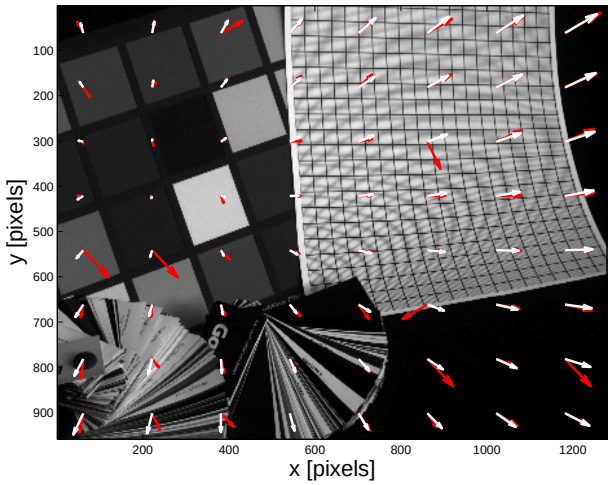

Figure 6: Scaled displacement vector field between channel 3 (500nm) and channel 4 (550nm), red: measurement data, white: model data, background: test image.

of the camera-internal filter. As both images were thus taken with the same camera-internal filter and without changing the imaging geometry, but with different illumination spectra, distortions between these images are mainly caused by chromatic aberrations, resulting in a pincushion-like displacement vector field [14]. Figure 7 shows the displacement vector field between the two images as estimated by our algorithm. Even though the vectors' maximum length is 0.14 pixel, we still observe a systematic displacement vector field consistent with what one expects from chromatic aberrations. Moreover, this confirms the ability of our registration algorithm to estimate displacements of down to one tenth of a pixel.

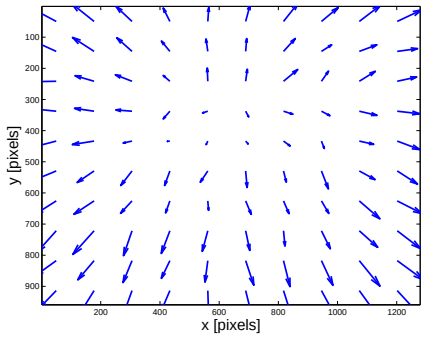

Figure 7: Measured displacement vector field (scaled) caused by chromatic aberration, maximum vector length: 0.14 pixel.

5. CONCLUSIONS

We have derived a mathematical model for the geometric distortion in filter wheel based multispectral cameras. Based on this model, we have developed a parametric registration algorithm to compensate these distortions. Apart from the filter-induced distortions, this algorithm also takes chromatic aberrations into account. Our experimental results on the one hand show that the geometric distortions are indeed compensated reliably, while on the other hand, they confirm the validity of the underlying model. An interesting question in this respect is inhowfar the optical filter parameters such as the angle γ, refraction index n_2 and the filter thickness d can be determined from the parameters of the estimated displacement vector field. This would enable the calibration of such cameras with respect to the filter parameters, and, vice versa, the prediction of the distortion fields obtained under different acquisition circumstances.

REFERENCES

[1] Cambridge Research & Instrumentation, Inc., http://www.cri-inc.com/.

[2] Spectral Imaging Ldt., http://www.specim.com.

[3] A.A. Bell, J.N. Kaftan, D. Meyer-Ebrecht and T. Aach, "An evaluation framework for the accuracy of camera transfer functions estimated from differently exposed images," in *IEEE SSIAI*, Denver, Colorado, Mar 26-28 2006, pp. 168–172.

[4] V. Cappellini, A. Del Mastio, A. De Rosa, A. Piva, A. Pelagotti and H. El Yamani, "An automatic registration algorithm for cultural heritage images," in *IEEE ICIP*, Genova, Italy, Sep 11-14 2005, pp. II–566-9.

[5] P. Colantoni, R. Pillay, C. Lahanier, and D. Pitzalis, "Analysis of multispectral images of paintings," in *Proc. EUSIPCO*, Florence, Italy, Sep 4-8 2006.

[6] M.A. Fischler and R.C. Bolles, "Random sample consensus: a paradigm for model fitting with applications to image analysis and automated cartography," in *Comm. ACM*, vol. 24(6), pp. 381–395, 1981.

[7] D.A. Forsyth and J. Ponce, *Computer Vision: A Modern Approach*, in Prentice Hall Professional Technical Reference, 2002.

[8] B.K. Gunturk, J. Glotzbach, Y. Altunbasak, R.W. Schafer, and R.M. Mersereau, "Demosaicking: color filter array interpolation," in *IEEE SPM*, vol. 22(1), pp. 44–54, Jan 2005.

[9] S. Helling, E. Seidel, and W. Biehlig, "Algorithms for spectral color stimulus reconstruction with a seven-channel multispectral camera," in *IS&Ts Proc. 2nd European Conf. CGIV*, Aachen, Germany, Apr 5-8 2004, pp. 254–258.

[10] F. König and P.G. Herzog, "On the limitation of metameric imaging," in *Proc. IS&Ts PICS*, vol. 2, pp. 163–168, 1999.

[11] R. Luther, "Aus dem Gebiet der Farbreizmetrik," in *Zeitschrift für technische Physik*, 8:540–558, 1927.

[12] F. Maes, A. Collignon, D. Vandermeulen, G. Marchal, and P. Suetens, "Multimodality image registration by maximization of mutual information," in *IEEE TMI*, vol. 16(2), pp. 187–198, 1997.

[13] J.P.W. Pluim, J.B.A. Maintz, and M.A. Viergever, "Mutual-information-based registration of medical images: a survey," in *IEEE TMI*, vol. 22(8), pp. 986–1004, Aug 2003.

[14] M. Rebiai, S. Mansouri, F. Pinson, and B. Tichit, "Image distortion from zoom lenses: modeling and digital correction," in *IBC*, Amsterdam, Netherlands, Jul 3-7 1992.